

ORIGINAL ARTICLE

Facile synthesis of chain-like LiCoO₂ nanowire arrays as three-dimensional cathode for microbatteries

Hui Xia^{1,2}, Yunhai Wan^{1,2}, Wilfried Assenmacher³, Werner Mader³, Guoliang Yuan¹ and Li Lu⁴

Three-dimensional microbatteries have emerged as a new direction for powering microelectronic devices, where the three-dimensional nanostructured electrode is the key component for microbatteries to achieve high power density and high energy density in a small footprint. In this work, we present a novel approach for fabrication of LiCoO₂ nanowire arrays as three-dimensional cathode for microbatteries. Mesoporous low-temperature LiCoO₂ nanowire arrays can be directly prepared by a two-step hydrothermal method and they can be easily converted into chain-like high-temperature LiCoO₂ nanowire arrays through further calcination. The layered LiCoO₂ nanowire arrays exhibit both high gravimetric capacity and areal capacity, while maintaining good cycling stability and rate capability. The facile synthesis and superior electrochemical performance of the three-dimensional LiCoO₂ cathode make it promising for application in microbatteries.

NPG Asia Materials (2014) 6, e126; doi:10.1038/am.2014.72; published online 19 September 2014

INTRODUCTION

Lithium-ion batteries with high energy density and design flexibility are the major power sources for portable electronic devices and are the promising candidates to power next generation of electric vehicles and hybrid electric vehicles.¹ However, to a much lesser degree have these advances benefitted the on-board power needs of microelectronics, another fast-growing market of billion dollar scale.² The recent advances in micro- or nanoelectromechanical systems have led to a variety of small-scale devices in microelectronics and biomedical area including microsensors, micromachines and drug delivery systems.³ To operate independently, these micro- or nano-electronic devices must have on-board power from power sources, which makes batteries the ideal power delivery choice. However, common rechargeable batteries based on the liquid electrolyte are not applicable due to the restrictions for on-chip design, size and inherent risk of leakage. Therefore, the need for all-solid-state thin-film microbatteries arises, which can facilitate miniaturization and create more flexibility for the design of stand-alone micro-/nano-electronic device.⁴

A key consideration for miniaturization, especially for integrated power, is the footprint area of the device. For thin-film microbattery designs with two-dimensional (2D) electrode geometries, there is areal footprint limitation as the total amount of stored energy for 2D batteries decreases because of the small electrode area. Making electrode thicker to store more energy is not a viable approach as the power density will be decreased as a result of prolonged Li-ion

diffusion length. The 2D battery design inherently imposes a compromise between energy density and power density for footprint-limited applications. Insufficient power from 2D microbattery configuration leads to the development of three-dimensional (3D) microbattery architecture, comprising a 3D matrix of components (cathode, anode and electrolyte) arranged in either a periodic array or an aperiodic ensemble to satisfy both the requirements of short transport lengths and large energy capacity.^{5,6}

The field of 3D microbatteries is poised for significant advances in the near future because of the development of a wide variety of synthesis techniques both for high-surface-area electrodes and for uniformly coating such electrodes with electrolyte layers. There are only a few reports on 3D microbatteries and most of them have been largely devoted to 3D-negative electrodes.^{7,8} 3D nanowire/nanotube arrays of negative electrodes have been successfully prepared, showing improved capacities and rate capabilities compared with their planar counterparts.^{9,10} However, there are very limited reports on the preparation of 3D-positive electrodes, which is probably due to the difficulty in synthesizing positive electrode arrays.^{11,12} LiCoO₂ is the most commonly used cathode material for lithium-ion batteries due to its excellent electrochemical performance and simple synthesis. LiCoO₂ exhibits two crystal structures depending on both the preparation method and the synthesis temperature. High-temperature (HT)-LiCoO₂ has a hexagonal layered structure, whereas the low-temperature (LT)-LiCoO₂ has a cubic spinel-related structure.¹³ Although there is one report on preparation of LiCoO₂

¹School of Materials Science and Engineering, Nanjing University of Science and Technology, Nanjing, China; ²Herbert Gleiter Institute of Nanoscience, Nanjing University of Science and Technology, Nanjing, China; ³Institute for Inorganic Chemistry, University of Bonn, Bonn, Germany and ⁴Department of Mechanical Engineering, National University of Singapore, Singapore, Singapore

Correspondence: Professor H Xia, School of Materials Science and Engineering, Nanjing University of Science and Technology, 200 Xiaolingwei, Nanjing, Jiangsu 210094, China.

E-mail: xiahui@njust.edu.cn

or Professor L Lu, Department of Mechanical Engineering, National University of Singapore, Singapore 117576, Singapore.

E-mail: luli@nus.edu.sg

Received 6 May 2014; revised 11 July 2014; accepted 15 July 2014

nanowire arrays using anodic aluminum oxide template, the quality of the arrays is unknown without showing any electrochemical performance.¹⁴ In the present work, a simple synthesis procedure was developed to prepare LT-LiCoO₂ and HT-LiCoO₂ nanowire arrays on Au and Ti substrates. The free-standing LT-LiCoO₂ nanowires exhibit a mesoporous structure whereas the HT-LiCoO₂ nanowires display a chain-like structure. The LT-LiCoO₂ and HT-LiCoO₂ nanowire arrays exhibit different electrochemical behaviors due to their different structural features. The 3D chain-like HT-LiCoO₂ nanowire arrays exhibit superior electrochemical performance, making them promising for application in 3D microbatteries.

EXPERIMENTAL PROCEDURES

Synthesis of LT- and HT-LiCoO₂ nanowire arrays

The LT-LiCoO₂ nanowire arrays were prepared by a two-step hydrothermal method. The general process is illustrated in Scheme 1 in detail. Ti and Au foils (about 1 cm²) were used as substrates to grow LiCoO₂ nanowire arrays. In step I, Co₃O₄ nanowire arrays were grown on the Ti and Au substrates by a common hydrothermal reaction according to our previous work.¹⁵ In a typical synthesis, 3 mmol of Co(NO₃)₂·6H₂O, 6 mmol of NH₄F and 15 mmol of CO(NH₂)₂ were dissolved in 30 ml of distilled water under continuous stirring. The obtained homogenous solution was transferred into Teflon-lined stainless steel autoclaves with metal substrates and heated at 120 °C for 5 h. After cooling down to room temperature, the substrates were rinsed with distilled water and calcinated at 400 °C in air for 4 h to obtain Co₃O₄ nanowire arrays. In step II, the lithiation to Co₃O₄ nanowire arrays was performed in a LiOH solution by another hydrothermal reaction. In a typical synthesis, 20 ml 2 M LiOH solution was prepared and transferred into a 30-ml Teflon-lined stainless steel autoclave with the metal substrate-supported Co₃O₄ nanowire arrays immersed into the solution. The autoclave was heated at 240 °C for 48 h to complete the lithiation. After cooling down to room temperature, the obtained LT-LiCoO₂ nanowire arrays grown on the metal substrates were rinsed with distilled water to remove the residuals of the reaction and dried in oven at 100 °C in air for further characterization. To prepare the HT-LiCoO₂ arrays, the Au or Ti substrate-supported LT-LiCoO₂ nanowire arrays were further calcinated at 750 °C in air for 2 h.

Structural and morphology characterization

The crystallographic information and phase purity of the products were investigated by X-ray diffraction (XRD; Shimadzu X-ray diffractometer 6000, Cu K_α radiation, Shimadzu, Tokyo, Japan), Raman spectroscopy (Jobin-Yvon T6400 Micro-Raman system, Jobin-Yvon, Villeneuve d'Ascq, France). The

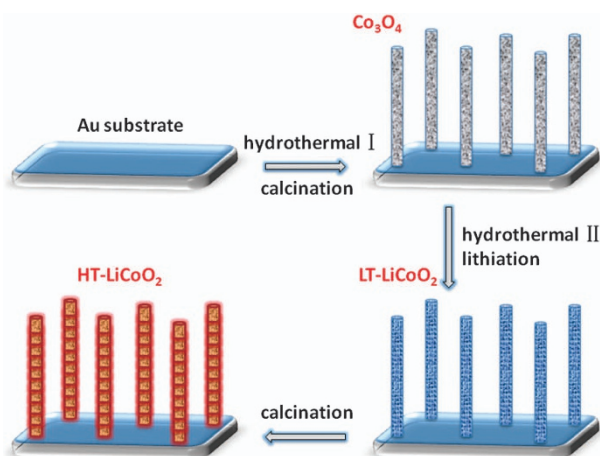
morphology and microstructure of the products were investigated by field emission scanning electron microscopy (FESEM; Hitachi S4300, Hitachi, Tokyo, Japan), transmission electron microscopy (TEM; FEI-Philips CM300 UT/FEG, FEI, Hillsboro, OR, USA) and high-resolution transmission electron microscopy (HRTEM). For TEM measurements, the nanowire samples were scratched from the Au substrates by doctor blade, dispersed in ethanol by ultrasonication, and finally casted on the TEM copper grids.

Electrochemical measurements

The Au or Ti substrates supported LT-LiCoO₂ and HT-LiCoO₂ nanowire arrays without any binders or conductive additives were directly used as the cathodes. Half cells using Li foil as both counter and reference electrodes were assembled with Lab-made Swagelok cells for the electrochemical measurements. In all, 1 M LiPF₆ in ethylene carbonate and diethyl carbonate (v/v = 1:1) solution was used as the electrolyte and Celgard 2400 was used as the separator. Cyclic voltammetry (CV) measurements were carried out in the voltage range between 3.0 and 4.2 V at a scan rate of 0.1 mV s⁻¹ using CHI660D (Shanghai Chenhua, Shanghai, China) electrochemical workstation. Galvanostatic charge and discharge measurements were carried out in the voltage range between 3.0 and 4.2 V at different C rates (1C = 148 mA g⁻¹) using LAND CT2001A electrochemical workstation at room temperature. Electrochemical impedance spectroscopy measurements were performed by applying an AC voltage of 5 mV in a frequency range between 0.01 Hz and 100 kHz at an open circuit potential. The mass loading of LiCoO₂ nanowires on the Au or Ti substrates is in the range of 0.3–0.5 mg cm⁻², which was measured by a Sartorius Analytical Balance (CPA225D, with a resolution of 10 μg, Sartorius, Goettingen, Germany).

RESULTS AND DISCUSSION

The phase purity and crystal structure of the products were investigated by XRD. Figure 1 shows the XRD spectra for the Au substrate, the Au substrate-supported Co₃O₄, LT-LiCoO₂ and HT-LiCoO₂ nanowire arrays, respectively. The XRD spectrum of the Au substrate (Figure 1a) is provided as a reference to differentiate the reflections of Au from the reflections of oxides for the other XRD spectra. Figure 1b shows the XRD spectrum of the Co₃O₄ nanowire arrays grown on the Au substrate, and all diffraction peaks from the oxide can be indexed to the cubic phase Co₃O₄ (JPCDS Card No. 42-1467), whereas Figure 1c shows the lithiated Co₃O₄ via LT hydrothermal processing, where two diffraction peaks from the oxide can be attributed to (111) and (222) reflections from the spinel LT-LiCoO₂



Scheme 1 Illustration of a facile two-step hydrothermal method for preparation of LT- and HT-LiCoO₂ nanowire arrays on metal substrates.

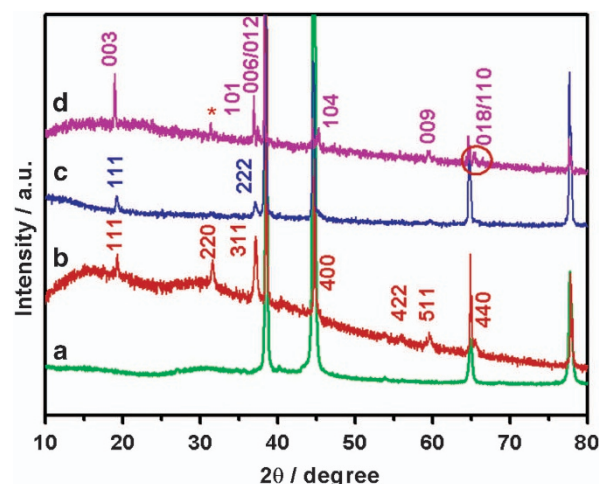


Figure 1 XRD spectra of (a) the Au substrate, the Au substrate-supported (b) Co₃O₄ nanowire arrays, (c) LT-LiCoO₂ nanowire arrays and (d) HT-LiCoO₂ nanowire arrays.

phase with Fd3m symmetry (JPCDS Card No. 74-1631). After further heat treatment, Figure 1d reveals most of diffraction peaks from oxide can be indexed to the layered HT-LiCoO₂ phase with R3-m symmetry (JPCDS Card No. 50-0653) with only one small peak assigned for Co₃O₄. As marked in a red circle in Figure 1d, the existence of (108)/(110) doublet clearly indicates the conversion from spinel to layered structure after the 750 °C heat treatment. The impurity peak can only be assigned to (220) reflection of Co₃O₄, which is probably induced by the lithium loss during the HT calcination. However, due to the strong Au diffraction peaks and similar XRD patterns for spinel and layered phases, it is difficult to confirm the formation of LT-LiCoO₂ and HT-LiCoO₂ by XRD results alone.

To further investigate the structure of the nanowire arrays grown on the Au substrates, Raman spectroscopy measurements were carried out on the different nanowire array samples. Figure 2 shows the Raman spectra of the Au substrate-supported Co₃O₄, LT-LiCoO₂ and HT-LiCoO₂ nanowire arrays, respectively. As shown in Figure 2a, there are three Raman bands located at 483, 523 and 623 cm⁻¹, which correspond, respectively, to the E_g, F_{2g}¹ and F_{2g}² modes of the crystalline Co₃O₄.¹⁶ Four Raman bands are observed in the Raman spectrum for LT-LiCoO₂ nanowire arrays at 430, 476, 580 and 598 cm⁻¹ (Figure 2b). The two higher frequency bands (580 and 598 cm⁻¹) can be assigned to Co-O stretching modes of the CoO₆ octahedra, while the two lower frequency bands (430 and 476 cm⁻¹) can be assigned to primarily O-Co-O bending motions.¹⁷ The presence of four bands in the Raman spectrum is strong evidence of spinel LT-LiCoO₂. For Figure 2c, there are only two Raman bands located at 481 and 591 cm⁻¹, which can be assigned to A_{1g} and E_g modes, respectively, indicating the presence of layered HT-LiCoO₂.¹⁸ The Raman results clearly confirm the structure transition from Co₃O₄ to LT-LiCoO₂ by lithiation and from LT-LiCoO₂ to HT-LiCoO₂ by HT calcination, agreeing well with the XRD results.

Figures 3a and b show the FESEM images of Co₃O₄ nanowire arrays grown on the Au substrate with low and high magnifications. It can be seen that bundled Co₃O₄ nanowire arrays are uniformly aligned on the Au substrate. With a sharp tip, each nanowire is about 100–200 nm in diameter. After hydrothermal lithiation, the morphology of the nanowire arrays does not change much as shown in Figures 3c and d. The enlarged FESEM image in Figure 3d shows that the

surface of the nanowires becomes coarse after lithiation, indicating a mesoporous structure. The FESEM results indicate that the hydrothermal lithiation will not change the nanowire morphology for the Co₃O₄ arrays and LT-LiCoO₂ nanowire arrays can be fabricated using the Co₃O₄ nanowire arrays as a template. As shown in Figure 3e, the nanowire morphology is still retained after calcination at 750 °C for 2 h, indicating the successful fabrication of HT-LiCoO₂ nanowire arrays. Figure 3f shows that the HT-LiCoO₂ nanowires have a highly porous structure with well-crystallized LiCoO₂ grains interconnected along the length direction, forming chain-like nanowire arrays on the Au substrate. However, further increasing the calcination temperature could destroy the morphology of the nanowires by forming randomly dispersed short nanorods (Supplementary Figure S1), which is probably due to further grain growth at higher temperature. Besides Au substrates, the LT-LiCoO₂ and HT-LiCoO₂ nanowire arrays can also be prepared on the Ti substrates with similar morphology (Supplementary Figures S2 and S3), which indicates this preparation method is applicable to various substrates. Figure 3g shows the TEM image of a single LT-LiCoO₂ nanowire. It can be seen that the LT-LiCoO₂ nanowire comprises closely packed nanograins of <50 nm in size, resembling a mesoporous structure. The inset in Figure 3g shows the Fast Fourier Transformation (FFT) image from the square area of a LiCoO₂ grain (Supplementary Figure S4), which can be indexed as cubic spinel in [111] zone axis orientation. Figure 3h shows the TEM image of three bundled HT-LiCoO₂ nanowires. Agreeing with the FESEM result, the chain-like structure is constructed by 100–200 nm LiCoO₂ grains connected by ends in length direction. Figure 3i shows the HRTEM image of one single crystal HT-LiCoO₂ grain with a Bragg-filtered HRTEM enlargement and FFT image of the square area. The indexing of the diffractogram shown in the FFT image succeeds only on the basis of the hexagonal metric of HT-LiCoO₂. The *d*-values measured in the HRTEM image and the power spectrum of 464 pm for {0003}, 228 pm for {-110-2} and 248 pm for {-1101} correspond well with the literature values of HT-LiCoO₂ within the experimental error.¹⁹ Single crystal electron diffraction patterns of trigonal HT-LiCoO₂ are also shown in the Supplementary Information (Supplementary Figure S5).

The LiCoO₂ nanowire arrays present a promising 3D cathode for microbatteries. Figures 4a and b show the typical CV curves for the LT-LiCoO₂ and HT-LiCoO₂ nanowire arrays, respectively, between 3 and 4.2 V at a scan rate of 0.1 mV s⁻¹. The CV curve for the LT-LiCoO₂ nanowire arrays exhibits one cathodic peak at 3.70 V and one anodic peak at 3.40 V, agreeing well with the CV behavior for the literature-reported LT-LiCoO₂.¹³ The large peak separation (~0.3 V) indicates a large cell polarization and large resistance of the cell. The CV curve for the HT-LiCoO₂ nanowire arrays exhibits one major cathodic peak and anodic peak at 3.93 and 3.89 V, and two minor cathodic peaks and anodic peaks at 4.08, 4.17 and 4.06, 4.15 V, respectively. The pair of major redox peaks correspond to the first-order phase transition, while the two pairs of minor redox peaks correspond to the order-disorder phase transitions.²⁰ Figure 4c shows the charge/discharge curves of the LT-LiCoO₂ nanowire arrays for the initial two cycles between 3 and 4.2 V at 0.1C rate. Agreeing well with the CV result, the charge/discharge curves show a 3.7-V plateau for the charge and a 3.4-V plateau for the discharge. The first charge and discharge capacities are 109 and 91 mAh g⁻¹, respectively, with a coulombic efficiency of about 83%. Figure 4d shows the charge/discharge curves of the HT-LiCoO₂ nanowire arrays for the initial two cycles between 3 and 4.2 V at 0.1C rate. One major voltage plateau at about 3.9 V and two minor voltage plateaus between 4 and 4.2 V are observed for both charge and discharge, which is consistent with the

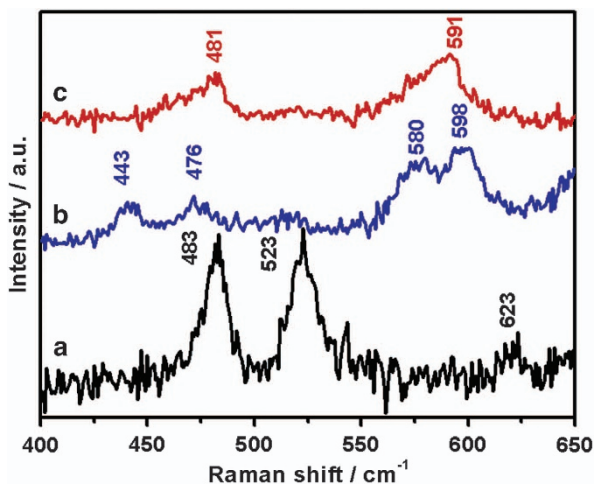


Figure 2 Raman spectra of the Au substrate-supported (a) Co₃O₄ nanowire arrays, (b) LT-LiCoO₂ nanowire arrays and (c) HT-LiCoO₂ nanowire arrays.

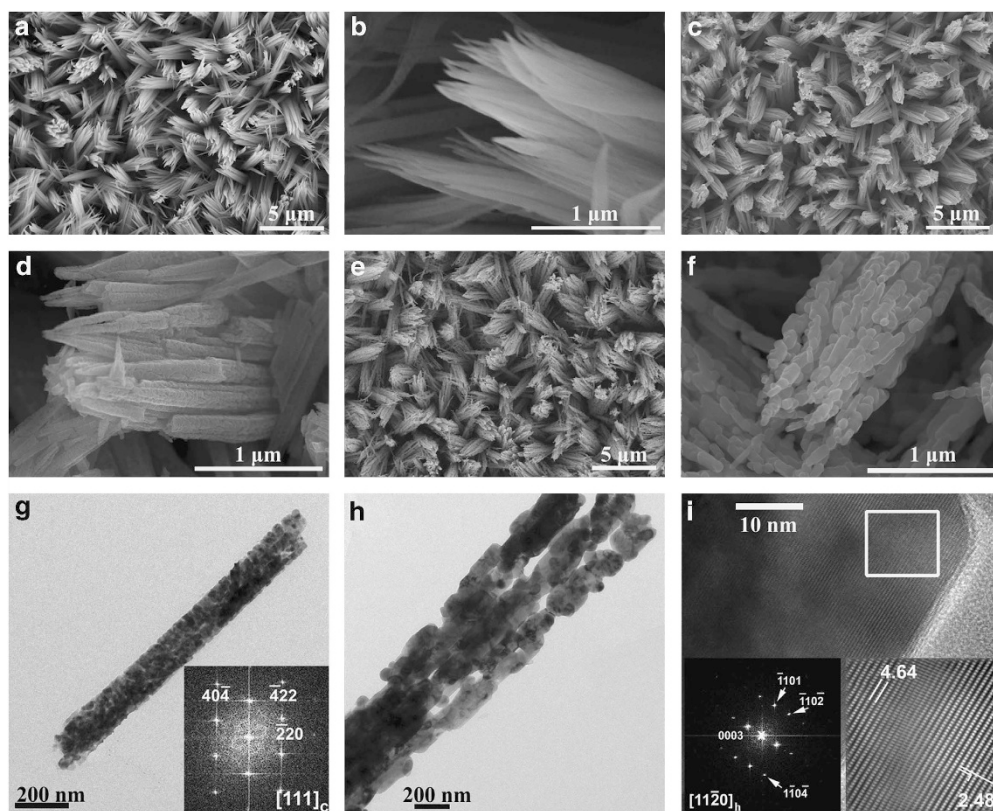


Figure 3 FESEM images of the (a, b) Co₃O₄ nanowire arrays, (c, d) LT-LiCoO₂ nanowire arrays and (e, f) HT-LiCoO₂ nanowire arrays. (g) TEM image of a single LT-LiCoO₂ nanowire (inset is an FFT image taken from one LT-LiCoO₂ grain). (h) TEM image of three bundled HT-LiCoO₂ nanowires. (i) HRTEM image of one HT-LiCoO₂ grain (left bottom inset is the FFT image taken from the square area and right bottom inset is the Fourier filtered enlargement of the square area).

CV result. The first charge and discharge capacities are 142 and 135 mAh g⁻¹, respectively, with a coulombic efficiency of about 95%. Prolong the hydrothermal reaction time will also lead to the conversion from LT-LiCoO₂ into HT-LiCoO₂ as the charge/discharge curves show both voltage plateaus for spinel and layered LiCoO₂ for the 72-h and 7-day samples (Supplementary Figures S6 and S7). However, the conversion is not complete and it takes too much time, which makes it not applicable for practical synthesis of HT-LiCoO₂ nanowire arrays. Although LiCoO₂ nanowire arrays grown on the Ti substrate show similar morphology as those grown on the Au substrate, their charge/discharge curves show much larger polarization with greatly reduced reversible capacity (Supplementary Figure S8), which is probably due to the formation of TiO₂ or other oxide layer on the surface of Ti substrate. Further increasing the hydrothermal temperature is dangerous since 240 °C is already the temperature limit for our autoclave system. It can be seen that the HT-LiCoO₂ nanowire arrays exhibit greatly improved reversibility for charge and discharge compared with the LT-LiCoO₂ nanowire arrays. Adhikary *et al.*²¹ proposed a model in which oxidation of divalent cobalt explains the charge/discharge irreversibility in the initial cycle for LT-LiCoO₂. Figure 4e shows the cycle performance of the LT-LiCoO₂ and HT-LiCoO₂ nanowire arrays at 0.1C rate for 50 cycles. After 50 cycles, the LT-LiCoO₂ and HT-LiCoO₂ nanowire arrays can retain 68 and 90% of their initial discharge capacities, respectively. The poor cycle performance of the LT-LiCoO₂ nanowire arrays could be attributed to the structural instability of quasi spinel structure on repeated extraction and reinsertion of lithium.¹³ In terms of reversible capacity and cycling stability, the HT-LiCoO₂ nanowire

arrays represent the more promising 3D cathode for Li-ion microbatteries. After the cycling test, the HT-LiCoO₂ nanowire array electrode was disassembled from the cell and further investigated by FESEM (Supplementary Figure S9). The self-supported nanowire morphology was well retained after the cycling test, which is due to the good structural stability of the layered LiCoO₂. This result indicates that the LiCoO₂ nanowire arrays have good adhesion to the Au substrate and such 3D architecture is stable during the cycling test. Moreover, the HT-LiCoO₂ nanowire arrays also exhibit excellent rate performance as shown in Figure 4f. Even at 10C rate, the HT-LiCoO₂ nanowire arrays can still deliver a very high reversible capacity of about 103 mAh g⁻¹, indicating high power capability.

Besides large gravimetric capacity, more importantly, the HT-LiCoO₂ nanowire arrays exhibit large areal capacity up to 0.27 mAh cm⁻², which is about 10 times larger than that of the 2D planar LiCoO₂ thin films.^{20,22} The areal capacity of the HT-LiCoO₂ nanowire arrays in the present work is also about two times larger than that of the previously reported Al nanorod-supported LiCoO₂ 3D electrode (~0.12 mAh cm⁻²),²³ which is probably due to the low loading of LiCoO₂ deposited on the Al nanorods. With excellent rate performance, the HT-LiCoO₂ nanowire arrays could provide both high energy density and high power density. The excellent rate performance could be attributed to the stable layered structure and the chain-like nanowire architecture of the HT-LiCoO₂ nanowire arrays. As shown in the inset Nyquist plot in Figure 4f, the electrochemical impedance spectroscopy spectrum of the HT-LiCoO₂ nanowire arrays shows a much smaller charge-transfer resistance

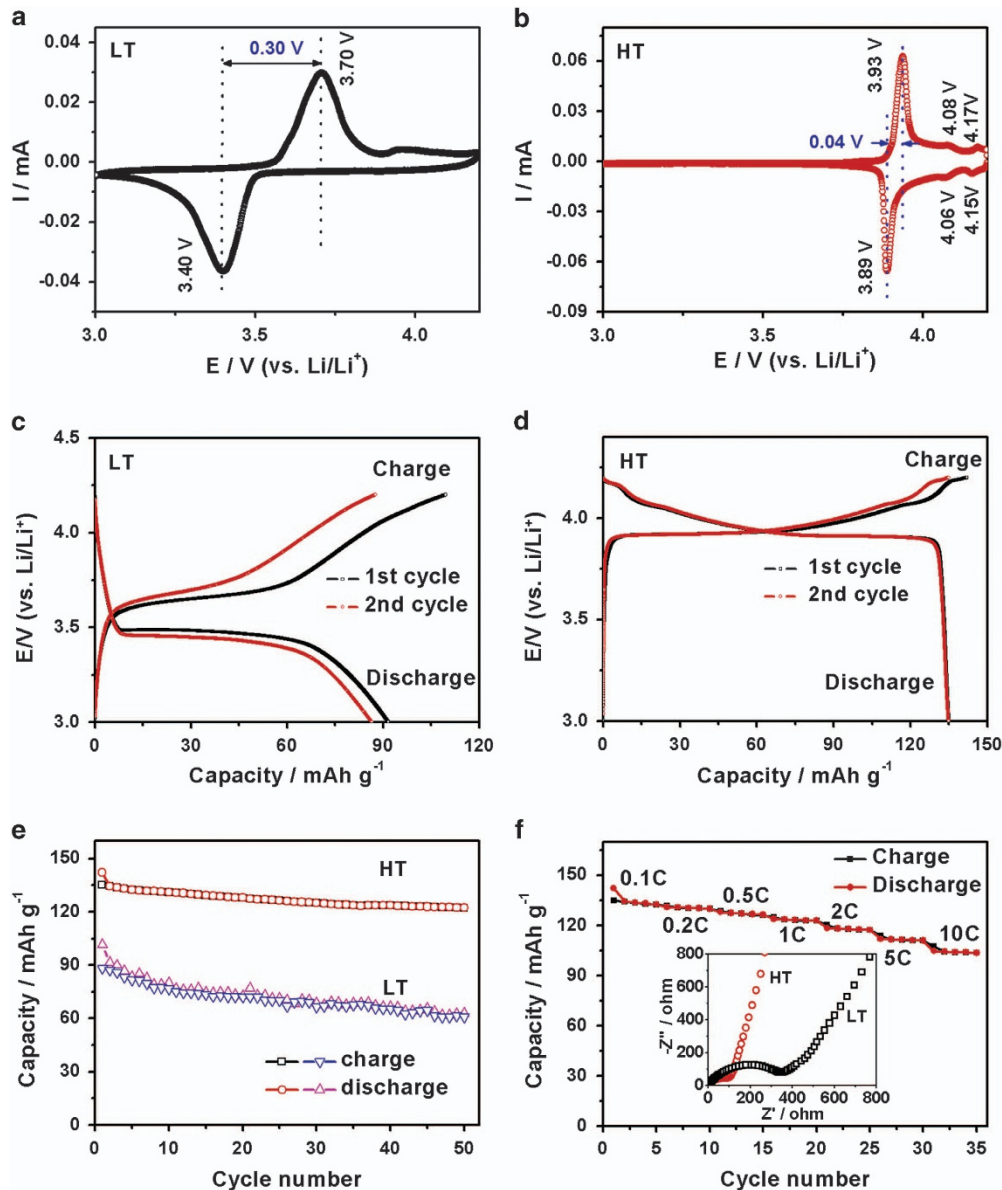


Figure 4 The typical CV curves for (a) the LT-LiCoO₂ nanowire arrays and (b) the HT-LiCoO₂ nanowire arrays between 3 and 4.2V at a scan rate of 0.1 mV s⁻¹. The initial two cycle charge/discharge curves for (c) the LT-LiCoO₂ nanowire arrays and (d) the HT-LiCoO₂ nanowire arrays between 3 and 4.2V at 0.1C rate. (e) Comparison of cycle performance between the LT-LiCoO₂ and HT-LiCoO₂ nanowire arrays. (f) Rate performance of the HT-LiCoO₂ nanowire arrays (inset is the Nyquist plot for the LT-LiCoO₂ and HT-LiCoO₂ nanowire arrays).

compared with that of the LT-LiCoO₂ nanowire arrays. The large charge-transfer resistance of the LT-LiCoO₂ nanowire arrays could explain the large charge/discharge irreversibility and poor Li-ion transport kinetics for the unstable quasi spinel structure. On the contrary, the stable layered structure provides fast Li-ion transport and high reversibility on repeated Li insertion and extraction. Moreover, the chain-like nanowire architecture facilitates fast electron transport along the length direction and the small LiCoO₂ grains shorten the Li-ion diffusion path with large surface area, thus enabling fast charge/discharge rates.

CONCLUSIONS

3D HT-LiCoO₂ and LT-LiCoO₂ nanowire arrays were, respectively, prepared on metal substrates by a facile two-step hydrothermal

method with or without calcination. The LT-LiCoO₂ nanowires present a mesoporous structure comprising very fine nanocrystallines, whereas the HT-LiCoO₂ nanowires exhibit a chain-like structure with larger grains connected by ends in the length direction. Although the LT-LiCoO₂ nanowire arrays have smaller grains, the HT-LiCoO₂ nanowire arrays exhibit larger capacity, better reversibility for charge/discharge and improved cycling stability, which can be attributed to the stable layered structure during repeated lithiation and delithiation. The current 3D electrode architecture provides both large surface area and shortened Li-ion diffusion length, thus enabling high energy density and power density in small footprint with excellent efficiency and stability. With facile preparation method, the HT-LiCoO₂ nanowire arrays can deliver a large areal capacity up to 0.27 mAh cm⁻², which is much larger than those of 2D planar

LiCoO₂ thin films and previously reported Al nanorod-supported LiCoO₂ arrays, making them promising as 3D cathode for the application in 3D microbatteries.

CONFLICT OF INTEREST

The authors declare no conflict of interest.

ACKNOWLEDGEMENTS

This work was supported by National Natural Science Foundation of China (Nos. 51102134 and 11134004), Natural Science Foundation of Jiangsu Province (No. BK20131349), China Postdoctoral Science Foundation (No. 2013M530258) and Jiangsu Planned Projects for Postdoctoral Research Funds (No. 1202001B).

Author contributions: HX designed and conceived the experiments. YW performed the experiments. WA and WM performed the TEM and data analysis. HX and LL co-wrote the manuscript.

- 1 Tarascon, J. M. & Armand, M. Issues and challenges facing rechargeable lithium batteries. *Nature* **414**, 359–367 (2001).
- 2 Arthur, T. S., Bates, D. J., Cirigliano, N., Johnson, D. C., Malati, P., Mosby, J. M., Perre, E., Rawls, M. T., Prieto, A. L. & Dunn, B. Three-dimensional electrodes and battery architectures. *MRS Bull.* **36**, 523–531 (2011).
- 3 Zhou, Y. N., Xue, M. Z. & Fu, Z. W. Nanostructured thin film electrodes for lithium storage and all-solid-state thin-film lithium batteries. *J. Power Sources* **234**, 310–332 (2013).
- 4 Oudenhoven, J. F. M., Baggetto, L. & Notten, P. H. L. All-solid-state lithium-ion microbatteries: a review of various three-dimensional concepts. *Adv. Energy Mater.* **1**, 10–33 (2011).
- 5 Dunn, B., Long, J. W. & Rolison, D. R. Rethinking multifunction in three dimensions for miniaturizing electrical energy storage. *Electrochem. Soc. Interface* **17**, 49–53 (2008).
- 6 Jiang, J., Li, Y. Y., Liu, J. P., Huang, X. T., Yuan, C. Z. & Lou, X. W. Recent advances in metal oxide-based electrode architecture design for electrochemical energy storage. *Adv. Mater.* **24**, 5166–5180 (2012).
- 7 Golodnitsky, D., Nathan, M., Yufit, V., Strauss, E., Freedman, K., Burstein, L., Gladkikh, A. & Peled, E. Progress in three-dimensional (3D) li-ion microbatteries. *Solid State Ionics* **177**, 2811–2819 (2006).
- 8 Pikul, J. H., Zhang, H. G., Cho, J., Braun, P. V. & King, W. P. High-power lithium ion microbatteries from interdigitated three-dimensional bicontinuous nanoporous electrodes. *Nat. Commun.* **4**, 1732 (2013).
- 9 Haag, J. M., Pattanaik, G. & Durstock, M. F. Nanostructured 3D electrode architectures for high-rate li-ion batteries. *Adv. Mater.* **25**, 3238–3243 (2013).
- 10 Wang, W., Tian, M., Abdulgatov, A., George, S. M., Lee, Y. C. & Yang, R. Three-dimensional Ni/TiO₂ nanowire network for high areal capacity lithium ion microbattery applications. *Nano Lett.* **12**, 655–660 (2012).

- 11 Gerasopoulos, K., Pomerantseva, E., McCarthy, M., Brown, A., Wang, C., Culver, J. & Ghodssi, R. Hierarchical three-dimensional microbattery electrodes combining bottom-up self-assembly and top-down micromachining. *ACS Nano* **6**, 6422–6432 (2012).
- 12 Liu, Y., Zhang, W., Zhu, Y., Luo, Y., Xu, Y., Brown, A., Culver, J. N., Lundgren, C. A., Xu, K., Wang, Y. & Wang, C. Architecturing hierarchical function layers on self-assembled viral templates as 3D nano-array electrodes for integrated Li-ion microbatteries. *Nano Lett.* **13**, 293–300 (2013).
- 13 Antolini, E. LiCoO₂: formation, structure, lithium and oxygen nonstoichiometry, electrochemical behaviour and transport properties. *Solid State Ionics* **170**, 159–171 (2004).
- 14 Zhou, Y., Shen, C. & Li, H. Synthesis of high-ordered LiCoO₂ nanowire arrays by AAO template. *Solid State Ionics* **146**, 81–86 (2002).
- 15 Xia, H., Zhu, D., Luo, Z., Yu, Y., Shi, X., Yuan, G. & Xie, J. Hierarchically structured Co₃O₄@Pt/MnO₂ nanowire arrays for high-performance supercapacitors. *Sci. Rep.* **3**, 2978 (2013).
- 16 Yu, T., Zhu, Y., Xu, X., Shen, Z., Chen, P., Lim, C. T., Thong, J. T. L. & Sow, C. H. Controlled growth and field-emission properties of cobalt oxide nanowalls. *Adv. Mater.* **17**, 1595–1599 (2005).
- 17 Burba, C. M., Shaju, K. M., Bruce, P. G. & Frech, R. Infrared and Raman spectroscopy of nanostructured LT-LiCoO₂ cathodes for Li-ion rechargeable batteries. *Vib. Spectrosc.* **51**, 248–250 (2009).
- 18 Tintignac, S., Baddour-Hadjean, R., Pereira-Ramos, Jean-Pierre & Salot, R. High performance sputtered LiCoO₂ thin films obtained at a moderate annealing treatment combined to a bias effect. *Electrochim. Acta* **60**, 121–129 (2012).
- 19 Xiao, X., Yang, L., Zhao, H., Hu, Z. & Li, Y. Facile synthesis of LiCoO₂ nanowires with high electrochemical performance. *Nano Res.* **5**, 27–32 (2012).
- 20 Xia, H., Lu, L., Meng, Y. S. & Ceder, G. Phase transitions and high-voltage electrochemical behavior of LiCoO₂ thin films grown by pulsed laser deposition. *J. Electrochem. Soc.* **154**, A337–A342 (2007).
- 21 Adhikary, K., Takahashi, M. & Kikkawa, S. Some new aspects of low-temperature lithium cobalt oxides prepared through citric acid precursor route. *Mater. Res. Bull.* **33**, 1845–1856 (1998).
- 22 Xia, H., Lu, L. & Ceder, G. Li diffusion in LiCoO₂ thin films prepared by pulsed laser deposition. *J. Power Sources* **159**, 1422–1427 (2006).
- 23 Shajumon, M. M., Perre, E., Daffos, B., Taberna, P. L., Tarascon, J. M. & Simon, P. Nanoarchitected 3D cathodes for li-ion microbatteries. *Adv. Mater.* **22**, 4978–4981 (2010).



This work is licensed under a Creative Commons Attribution-NonCommercial-ShareAlike 3.0 Unported License. The images or other third party material in this article are included in the article's Creative Commons license, unless indicated otherwise in the credit line; if the material is not included under the Creative Commons license, users will need to obtain permission from the license holder to reproduce the material. To view a copy of this license, visit <http://creativecommons.org/licenses/by-nc-sa/3.0/>

Supplementary Information accompanies the paper on the NPG Asia Materials website (<http://www.nature.com/am>)